Heat percolation in many-body flat-band localizing systems

Ihor Vakulchyk,[1,2,*] Carlo Danieli,[3,†] Alexei Andreanov,[1,2,‡] and Sergej Flach[1,2,§]

[1]*Center for Theoretical Physics of Complex Systems, Institute for Basic Science (IBS), Daejeon 34126, Republic of Korea*

[2]*Basic Science Program, Korea University of Science and Technology (UST), Daejeon 34113, Republic of Korea*

[3]*Max Planck Institute for the Physics of Complex Systems, Dresden D-01187, Germany*

(Received 3 June 2021; revised 9 September 2021; accepted 6 October 2021; published 27 October 2021)

We demonstrate robust ergodicity breaking in interacting many-body systems in arbitrary Euclidian dimension based on disorder-free many-body localization. Translationally invariant fine-tuned single-particle lattice Hamiltonians can host dispersionless (flat) bands only. Suitable short-range many-body interactions enforce complete suppression of particle transport due to local constraints and lead to ergodicity breaking termed many-body flat-band localization. However, heat might still flow between spatially locked charges. We demonstrate that heat transport is completely suppressed in one dimension. In higher dimensions we establish a universal bound on the filling fraction below which the heat transport is suppressed. The bound is based on the mapping to a classical percolation problem. Above the bound, the heat transport in percolation clusters is additionally affected by emerging bulk disorder and edge scattering induced by local constraints, which work in favor of arresting the heat flow and might keep the ergodicity breaking above the universal bound. We discuss explicit examples in one and two dimensions.

DOI: 10.1103/PhysRevB.104.144207

Introduction. The breaking of ergodicity in interacting quantum many-body systems is an important open problem and active topic of research. One example is many-body localization (MBL): The first studies [1–5] showed that MBL and the exponential suppression of any transport arise in one-dimensional (1D) interacting systems from the interplay of random fields and interactions. While the original MBL framework has been widely developed both theoretically and experimentally [6,7], the need for random fields as a key element for MBL has been later relaxed, and alternative mechanisms for ergodicity breaking were proposed, e.g., disorder-free MBL and Hilbert space shattering. Indeed, MBL features have been observed in a variety of systems without disorder [8–13]—particularly in interacting systems featuring an extensive number of local constraints [14–19]. Computationally, interacting quantum systems face an exponential divergence in complexity over the system size, which limits most numerical efforts to one dimension. This, and the lack of analytically treatable models and methods, renders the crucial quest for ergodicity breaking in higher-dimensional networks particularly challenging. Indeed, while signatures of MBL in 2D systems have been reported [20,21], and results from the avalanche framework [22,23] indicate persistence of the transition in larger dimensions [24], it has also been shown that in $D > 1$ the MBL regime is possibly unstable and destabilized in the long-time limit [25].

In this paper, we study the transport features of disorder-free many-body systems with ergodicity breaking which are based on Hamiltonian networks completely lacking single-particle dispersion. In particular, we relate the existence of a phase transition between conducting and insulating regimes to the lattice profile and its dimensionality. In translationally invariant lattices, the lack of single-particle dispersion in, e.g., one Bloch band typically results in the presence of a macroscopically degenerate set of *compact localized states* (CLSs)—spatially compact eigenstates [26–28]. Hence a complete lack of dispersion—i.e., when all Bloch bands are flat, referred to as "all bands flat" (ABF) [29–31]—results in the absence of extended states and strict single-particle confinement in the network. Flat-band networks are increasingly permeating the quantum many-body field. Indeed, single-particle CLSs have been extended to many-body CLSs [32–34], while quantum scars [35–37] and MBL-like dynamics [38–40] have been reported very recently in flat-band lattices. However, more importantly, it has been shown that fine-tuning of the interaction in ABF networks induces an extensive set of local constraints which completely suppress charge transport in any spatial dimension—a phenomenon called many-body flat-band localization (MBFBL) [41–43]. While MBFBL models originate from a fine-tuning protocol (see Ref. [41] for details) which makes them conceptually different with respect to conventional MBL systems, they offer an innovative platform to study novel quantum ergodicity breaking phenomena. In this paper, by recasting MBFBL networks into a site-percolation problem we demonstrate the robustness of the ergodicity-broken phase up to a certain filling fraction, similar to the results obtained in Ref. [19] for a different model. Our main finding is a universal lower bound on the critical filling fraction that depends only on

*Corresponding author: igrvak@gmail.com

†Corresponding author: cdanieli@pks.mpg.de

‡Corresponding author: aalexei@ibs.re.kr

§Corresponding author: sergejflach@googlemail.com

dimensionality and lattice geometry, but not on the details of the Hamiltonian. More specifically, the transition is absent, and any transport is suppressed in all such 1D networks, whereas in $D \geqslant 2$ the presence of the transition is bounded by the MBFBL geometry—highlighting high-dimensional many-body systems where transport vanishes at any filling fraction. However, we note that in the conducting phase above the bound predicted by percolation theory, the local constraints might hurdle this and potentially stop transport by generating effective bulk and edge disorders. Furthermore, these disorders are nonuniversal and depend on the microscopic details of the Hamiltonian.

Setup. We study interacting many-body systems whose Hamiltonians consist of D-dimensional networks with ν strictly flat energy bands equipped with fine-tuned two-body interactions. We consider spinless fermions, and following the scheme outlined in Ref. [41], we focus on a set of Hamiltonians written as

$$\hat{\mathcal{H}} = \hat{\mathcal{H}}_{\rm sp} + V\hat{\mathcal{H}}_{\rm int} = \sum_{\mathbf{l}} \hat{C}_{\mathbf{l}}^{\dagger T} H_0 \hat{C}_{\mathbf{l}} + V \sum_{\langle \mathbf{l}_1, \mathbf{l}_2 \rangle} \sum_{a,b} J_{a,b}^{\mathbf{l}_1,\mathbf{l}_2} \hat{n}_{\mathbf{l}_1,a} \hat{n}_{\mathbf{l}_2,b}, \tag{1}$$

where in $\hat{\mathcal{H}}_{\rm sp}$ the fermionic annihilation (creation) operators $\hat{c}_{\mathbf{l},a}$ ($\hat{c}_{\mathbf{l},a}^{\dagger}$) have been grouped in ν-dimensional vectors $\hat{C}_{\mathbf{l}}$ ($\hat{C}_{\mathbf{l}}^{\dagger}$), while H_0 is a Hermitian matrix, $\mathbf{l}$ is a D-dimensional multi-index, and a, b label sites in unit cells. In Ref. [41], this representation of $\hat{\mathcal{H}}_{\rm sp}$ has been named *semidetangled* since $\hat{\mathcal{H}}_{\rm sp}$ consists of decoupled unit cells of ν lattice sites each, whose profile is defined by H_0. The interaction $\hat{\mathcal{H}}_{\rm int}$ is set as products of particle-number operators $\hat{n}_{\mathbf{l},a} = \hat{c}_{\mathbf{l},a}^{\dagger}\hat{c}_{\mathbf{l},a}$. The multi-indices $\langle \mathbf{l}_1, \mathbf{l}_2 \rangle$ account for neighboring unit cells reflecting the geometry of the interaction network, while the coefficients $J_{a,b}^{\mathbf{l}_1,\mathbf{l}_2}$ define the interaction between cells $\mathbf{l}_1$ and $\mathbf{l}_2$.

The addition of a fine-tuned density-density interaction $\hat{\mathcal{H}}_{\rm int}$ to the semidetangled all-band-flat networks $\hat{\mathcal{H}}_{\rm sp}$ in Eq. (1) results in strict particle localization—a phenomenon labeled many-body flat-band localization (MBFBL) [41]. Indeed, the local operators $\hat{I}_{\mathbf{l}} = \sum_{a=1}^{\nu} \hat{n}_{\mathbf{l},a}$, which count the number of particles within each unit cell, commute with $\hat{\mathcal{H}}$ (1) and prohibit charge transport. The Hilbert space decomposes into dynamically independent subspaces characterized by the eigenvalues of $\{\hat{I}_{\mathbf{l}}\}$. In general, the local conserved quantities $\hat{I}_{\mathbf{l}}$ do not forbid global heat transport, since particles confined to neighboring unit cells might still exchange energy locally via the interaction $\hat{\mathcal{H}}_{\rm int}$ [44]. However, the local heat exchange vanishes if at least one of the two cells coupled by $\hat{\mathcal{H}}_{\rm int}$ is either empty or full, i.e., $\hat{I}_{\mathbf{l}} = \{0, \nu\}$. Consequently, unit cells of Eq. (1) split according to their occupation number into *blocking* (empty or full cell, $\hat{I}_{\mathbf{l}} = \{0, \nu\}$) or *nonblocking* (all other cases, $\hat{I}_{\mathbf{l}} \neq \{0, \nu\}$). The impact of blocking cells on the global heat transport in Eq. (1) depends on the network geometry encoded by $\langle \mathbf{l}_1, \mathbf{l}_2 \rangle$, its spatial dimension D, the number of single-particle flat bands ν, and the filling fraction δ.

One-dimensional case. In 1D MBFBL networks (1), a single blocking unit cell acts as a bottleneck, strictly disconnecting the left and right parts of a given state of the Hilbert space and completely removing any global heat transport. Consequently, subspaces labeled by $\{\hat{I}_l\}$ are separated into (i) *nonblocked channels*, where every unit cell is nonblocked [hence there exists a continuous path of unblocked (heat-exchanging) units which connect opposite ends of the system], and (ii) *nonconducting states*, where at least one unit cell is blocking. Within a nonconducting state, blocking cells separate contiguous nonblocking unit cells, *nonblocked islands*, where heat transport might be possible although nonglobal. We remark, however, that the presence of continuous paths of nonblocking or heat-exchanging units in nonblocked channels might not be sufficient to allow for transport in the corresponding subspace. The existence of nonblocked channels—and the possibility of heat transport—in 1D networks (1) is controlled by the filling fraction δ. For $1/\nu \leqslant \delta \leqslant (\nu - 1)/\nu$, nonblocked and nonconducting channels coexist; otherwise only nonconducting states are present.

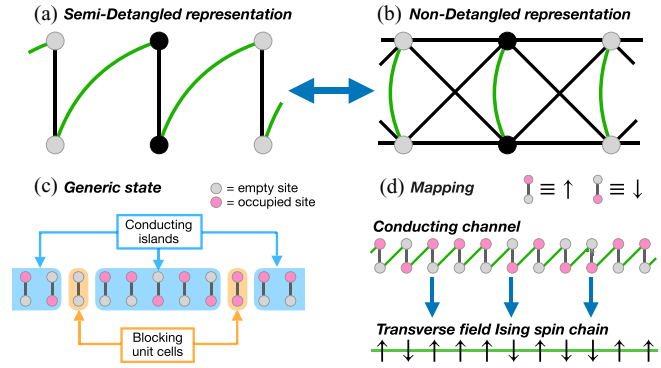

FIG. 1. (a) One-dimensional $\nu = 2$ MBFBL network, Eq. (2), with $\hat{\mathcal{H}}_{\rm sp}$ (black lines) and $\hat{\mathcal{H}}_{\rm int}$ (green curves). The black circles indicate the unit cell choice. (b) Same as (a) with $\hat{\mathcal{H}}_{\rm sp}$ nondetangled (cross-stitch). (c) Nonblocked islands (blue shaded areas) and blocking unit cells (orange shaded areas) in a generic state of the Hilbert space of $\hat{\mathcal{H}}$. (d) Visualization of the mapping of $\hat{\mathcal{H}}$ (2) to a transverse field Ising spin chain $\hat{\mathcal{H}}^I$ (3) in the subspace of nonblocked channels at $\delta = 0.5$. The green horizontal line indicates the spin-interaction terms.

The $\nu = 2$ case is the minimal test-bed setup. In this case, nonblocked channels are only present at exactly filling fraction $\delta = 0.5$ ($\hat{I}_l = 1$ in all cells). An example network (1) is shown in Fig. 1(a); the corresponding Hamiltonian $\hat{\mathcal{H}}$ reads

$$\hat{\mathcal{H}} = \sum_l (\hat{a}_l, \quad \hat{b}_l)^{\dagger} \begin{pmatrix} s & t \\ t & s \end{pmatrix} \begin{pmatrix} \hat{a}_l \\ \hat{b}_l \end{pmatrix} + V \sum_l \hat{n}_{b,l}\hat{n}_{a,l+1}, \tag{2}$$

where $\hat{a}_l, \hat{b}_l$ ($\hat{a}_l^{\dagger}, \hat{b}_l^{\dagger}$) are the fermionic annihilation (creation) operators, $\hat{n}_{a,l}, \hat{n}_{b,l}$ are the respective particle-number operators, and s, t are on-site energies and intracell hopping, respectively. Note that this network is related to the (nondetangled) cross-stitch lattice in Fig. 1(b) by local unitary transformations [45], which preserve $\hat{\mathcal{H}}_{\rm int}$ as a density-density interaction [41].

A generic nonconducting state is shown in Fig. 1(c), where nonblocked islands are separated by blocking unit cells. Instead, a sample nonblocked channel is shown in Fig. 1(d). Within such channels that exist at $\delta = 0.5$, the Hamiltonian $\hat{\mathcal{H}}$ (2) maps onto a spin-$\frac{1}{2}$ transverse field Ising model [46]. The mapping is visualized in Fig. 1(d): We define local spin basis $|\uparrow\rangle \equiv \hat{a}_l|0\rangle$ (one fermion at site a) and $|\downarrow\rangle \equiv \hat{b}_l|0\rangle$ (one fermion at site b) for each unit cell l. In this representation, the

on-site terms of $\hat{\mathcal{H}}$ become an identity, the hopping terms turn into σ_l^x, and the interaction reads $(1-\hat{\sigma}_l^z)(1+\hat{\sigma}_{l+1}^z)/4$, where $\hat{\sigma}_l^\alpha$ are Pauli matrices. The effective spin-$\frac{1}{2}$ Hamiltonian of the conducting channels reads

$$\hat{\mathcal{H}}_{\rm I} = t\sum_l \hat{\sigma}_l^x - \frac{V}{4}\sum_l \hat{\sigma}_l^z\hat{\sigma}_{l+1}^z + \frac{V}{4}\left(\hat{\sigma}_L^z - \hat{\sigma}_1^z\right), \qquad (3)$$

where the last term vanishes for periodic boundary conditions [47]. Note that this mapping also holds within individual nonblocked islands of nonconducting channels. In that case, the boundary term in Eq. (3) depends on whether the blocking cells at the edges of the island are empty or filled [48].

This mapping of $\hat{\mathcal{H}}$ (2) to the transverse field Ising chain $\hat{\mathcal{H}}_{\rm I}$ (3) shows globally ballistic heat transport in the nonblocked channel [49]. However, this does not imply that Eq. (2) necessarily supports ballistic transport. In fact, the nonblocked channel is a strict subset of the full Hilbert space of Eq. (2), and the total dimension of nonconducting channels overpowers the dimension of the nonblocked channels for diverging number L of unit cells. Indeed, the size of the nonblocked channel is 2^L, while the full Hilbert space dimension is $\mathcal{D} = \binom{2L}{L} \sim 2^{2L}/\sqrt{L}$ for large L. Consequently, the relative dimension $\mathcal{R}$ of the nonblocked channel with respect to the full Hilbert space $\mathcal{D}$ is $\mathcal{R} \sim 2^{-L}\sqrt{L}$, implying an exponential suppression of heat transport for large L. Note that the eigenenergies of the conducting subspace are spread throughout the entire spectrum. These results are not specific to the test-bed case, Eq. (2), but apply to any choice of $\hat{\mathcal{H}}_{\rm sp}$ and $\hat{\mathcal{H}}_{\rm int}$ in $\hat{\mathcal{H}}$ in Eq. (1) that leads to MBFBL.

In general, for $\nu \geqslant 3$, nonblocked channels are present if and only if the filling fraction is within the range $1/\nu \leqslant \delta \leqslant (\nu-1)/\nu$. Similarly to the $\nu = 2$ case, the ratio $\mathcal{R}$ between the dimension of the nonblocked channels and the full Hilbert space dimension decays exponentially in L, with the decay rate depending on the number of bands and the filling fraction. For example, for $\nu = 3$ this ratio scales as

$$\mathcal{R} \sim \left\{\frac{(\delta-1/3)^{\delta-1/3}(2/3-\delta)^{2/3-\delta}}{\delta^\delta(1-\delta)^{1-\delta}}\right\}^{-3L}, \qquad (4)$$

where the expression in the braces is strictly larger than 1 for any $1/3 \leqslant \delta \leqslant 2/3$. Otherwise nonblocked channels are completely absent.

For $\nu = 3$ systems (1), nonblocked channels are given by $\hat{I}_l = 1, 2\ \forall l$; namely, each unit cell contains either one or two fermions. This corresponds to three degrees of freedom per unit cell, leading to a mapping onto a spin-1 model. However, the matrix H_0 in (1), which translates into local fields, is different for singly or doubly occupied cells [50]. Similarly, the mapping of the interaction $\hat{\mathcal{H}}_{\rm int}$ depends on the filling fraction of the neighboring unit cells $\hat{I}_l, \hat{I}_{l+1}$. Consequently, an inhomogeneous distribution of charges in the nonblocked channel generates an effective disorder in the interaction terms of the effective spin-1 Hamiltonian, and, possibly, in its local field components (according to H_0). Such effects also persist for $\nu \geqslant 4$ networks, where in addition to the disorder in local fields and the interactions, different possible fillings of the unit cells $1 \leqslant \hat{I}_l \leqslant \nu - 1$ produce spins of different lengths—generating an effective disorder in the spin lengths. All these effective disorders might hinder and potentially halt transport in nonblocked channels: It has been shown that disorder in the interactions also can induce MBL [51]. This mapping is illustrated in Fig. 2(b) for a sample MBFBL network that extends Eq. (2) to $\nu = 3$. The details of the mapping are schematically represented in Fig. 2(a), where black and red colors indicate the different field components of H_0. The resulting transformation from a sample nonblocked channel to a spin chain is visualized in Fig. 2(c), where the green and magenta horizontal lines indicate different interaction operators.

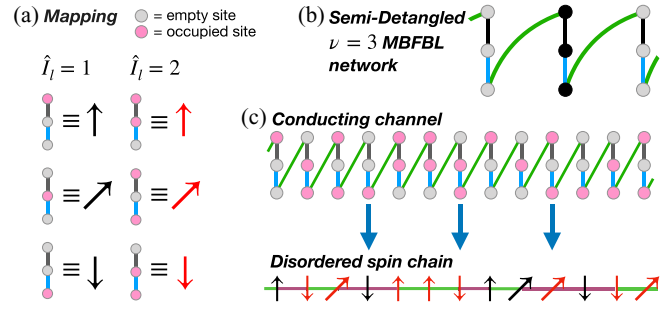

FIG. 2. (a) Mapping of nonblocking unit cells to spin-1 representation of $\nu = 3$ MBFBL networks separated in $\hat{I}_l = 1$ and $\hat{I}_l = 2$. Black and red colors indicate different spin field components. (b) One-dimensional sample $\nu = 3$ MBFBL network, Eq. (1), represented in the same way as in Fig. 1(a). Blue and black lines indicate two different hoppings. (c) Recasting a nonblocked channel into spin representation via the mapping in (a). Green and magenta horizontal lines represent the spin-interaction terms between neighboring unit cells with the same value or different values of $\hat{I}_l$, respectively.

Higher dimensions. Unlike the one-dimensional case, a single blocking unit cell is not a bottleneck and does not completely halt global transport in $D \geqslant 2$. Thus a subspace is a *nonblocked channel* if there is at least one path formed by nonblocking cells connecting opposite ends of the network. Otherwise, a subspace is nonconducting. For finite system sizes, non-blocked channels exist only in a limited range of filling fractions δ, which converges to the full available interval $0 < \delta < 1$ for $L \to \infty$; for example, for a square lattice of size L, nonblocked channels exist for $1/(\nu L) \leqslant \delta \leqslant (\nu L - 1)/(\nu L)$. In the infinite-system-size limit, let us consider a random state from the particle-number basis. The probability p for a given unit cell in the state to be nonblocking (e.g., neither empty, $\hat{I}_l = 0$, nor full, $\hat{I}_l = \nu$) is $p = 1 - \delta^\nu - (1-\delta)^\nu$. However, because the sampling is performed from the fermionic Hilbert space basis, the events of each of the unit cells being nonblocking are correlated. However, these correlations are inversely proportional to the system size and become negligible as $L \to \infty$ (as we verify numerically below). Therefore counting the relative dimension of nonblocked channels $\mathcal{R}$ with respect to the size of the Hilbert space in a network (1) is equivalent to a site-percolation problem, which is covered by the standard Bernoulli percolation theory [52]. In the site-percolation problem there exists always a critical value of probability $p_{\rm cr}$ [53] which depends on the network geometry, such that $\mathcal{R} \xrightarrow[L\to\infty]{} 0$ for $p < p_{\rm cr}$ (*nontransporting* regime) while $\mathcal{R} \xrightarrow[L\to\infty]{} 1$ for $p > p_{\rm cr}$ (*nonblocked* regime) [54].

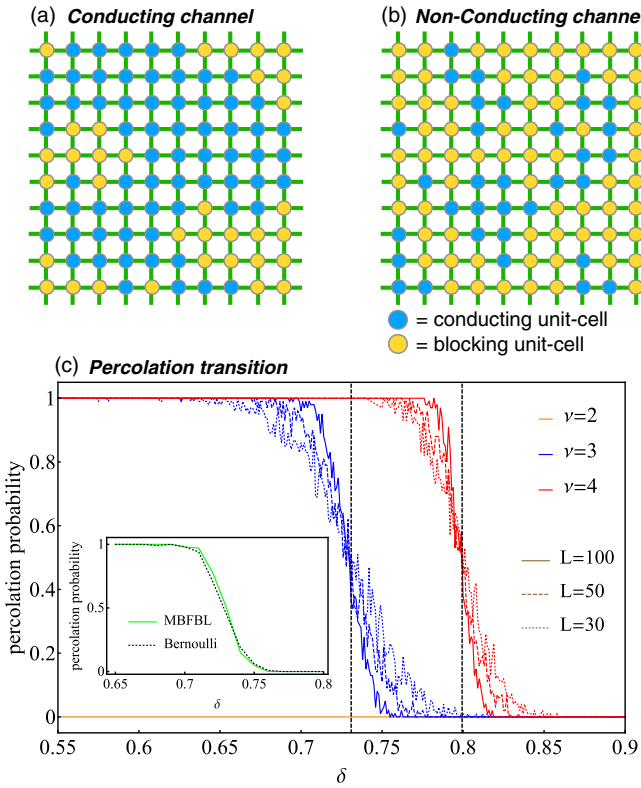

FIG. 3. (a) Typical state from a nonblocked channel in an equispaced square MBFBL network, Eq. (1), with fully detangled $\hat{\mathcal{H}}_{\rm int}$ (green lines) and semidetangled $\hat{\mathcal{H}}_{\rm sp}$ (circles) distinguished in nonblocking unit cells (blue) and blocking unit cells (yellow). (b) Same as (a) for a nonconducting subspace. (c) Percolation probability vs filling fraction δ for different system sizes L and numbers of sites per unit cell ν calculated using 100 Monte Carlo samples for each point. Vertical dashed lines indicate the critical filling fraction given by Eq. (5). Inset: Comparison of Bernoulli and MBFBL percolation models for $\nu = 3, L = 100$.

In the MBFBL networks (1), the critical transition probability $p_{\rm cr}$ depends on the network connectivity $\langle \mathbf{l}_1, \mathbf{l}_2 \rangle$ that links the detangled unit cells, together with the dimensionality D. Instead, the particular choices of the matrix H_0 and interaction coefficients $J_{a,b}^{\mathbf{l}_1,\mathbf{l}_2}$ in Eq. (1) are irrelevant for $p_{\rm cr}$ (so long as the network connectivity is unchanged). The critical values of the filling fraction $\delta_{\rm cr}$ where a transition between nontransporting and nonblocked regimes occurs are related to the critical probability $p_{\rm cr}$ through

$$1 - \delta_{\rm cr}^{\nu} - (1 - \delta_{\rm cr})^{\nu} = p_{\rm cr}. \tag{5}$$

We start with the simplest case and consider a $D = 2$ Hamiltonian $\hat{\mathcal{H}}$ (1) arranged as a square lattice. In Fig. 3 we schematically illustrate nonblocked channels [Fig. 3(a)] and states from nonconducting subspace [Fig. 3(b)]. The site-percolation critical value in this network is $p_{\rm cr} \sim 0.59$ [55]. In Fig. 3(c) we show the numerically computed percolation probability as a function of the filling fraction δ for several system sizes L and numbers of sites per unit cell ν. The inset of Fig. 3(c) compares the percolation probabilities calculated from the Bernoulli percolation model and from the direct sampling of the fermionic Hilbert space. The results are in excellent agreement, thus justifying the application of the Bernoulli model. For $\nu = 2$ the probability that a unit cell is nonblocking is $p \leqslant 0.5$ for any δ, with the maximum $p = 0.5$ being reached at $\delta = 0.5$; hence the transition value $p_{\rm cr} \sim 0.59$ is never reached, the network never undergoes percolation transition, and global transport is suppressed for all filling fractions δ. Numerical simulations confirm this conclusion for $\nu = 2$. For $\nu = 3, 4$, numerical simulations give clear evidence of a percolation transition upon varying δ, again in excellent agreement with the critical values predicted by Eq. (5).

In $D = 2$ the majority of lattices—kagome, honeycomb, and octagon—have critical values $p_{\rm cr} \gtrless 0.5$ [56]. Exceptions include networks with further than nearest-neighbor terms [57], chimera [58], and triangular lattices [59]. Hence, in two dimensions, most $\nu = 2$ MBFBL networks $\hat{\mathcal{H}}$ avoid percolation transition (and therefore any transport is absent) since the maximum probability of a unit cell to be nonblocking is $p = 0.5$. As D increases, the critical transition $p_{\rm cr}$ in a given class of lattices typically decreases: For example, $D \geqslant 3$ hypercubic network $\hat{\mathcal{H}}$ percolation transition occurs for any $\nu \geqslant 2$ [53]. However, there are exotic networks on which $\hat{\mathcal{H}}$ avoid percolation transition: For instance, $\nu = 2$ MBFBL networks on 3D cubic oxide or 3D silicon dioxide [60,61].

Geometric percolation theory yields regions of filling fraction where the number of states from nonblocked channels is dominating over those from the nonconducting ones. However, such results do not account for quantum effects following the distribution of the local constraints $\{\hat{I}_{\mathbf{l}}\}$. Such effects include the following: (i) disorder in the interaction terms, the local spin fields (for $\nu \geqslant 3$), and the spin lengths (for $\nu \geqslant 4$), as explained for 1D networks; (ii) edge scattering, as percolating clusters have in general a highly irregular fractal structure [62] (effect already present in classical percolation, although further amplified by the inhomogeneous arrangements of $\{\hat{I}_{\mathbf{l}}\}$); and (iii) possible dead-end bonds, which fully reflect wave transmission. Such effects may potentially hinder and halt transport in the percolating regimes of Eq. (1). Whether they lead to an effective increase in the percolation threshold with respect to the classical one for MBFBL networks obtained via Eq. (5)—a phenomenon called *quantum percolation* [63,64]—is one of the yet open issues that needs to be faced in future works.

Conclusions and perspectives. In this paper we studied transport features of translationally invariant interacting many-body flat-band localization (MBFBL) networks [41–43]. While charges are strictly confined in these models due to local constraints, heat is in principle allowed to flow along nonblocked channels—leading to a mapping onto site-percolation problems. We found that in one dimension the number of nonblocked channels either vanishes or decays exponentially with the system size, hence always suppressing any transport in the thermodynamic limit. In higher dimensions, the number of nonblocked channels can undergo a percolation transition upon tuning the filling fraction δ, providing a lower bound for the potential heat transport. The presence of the transition depends on the network type, the number of single-particle energy bands ν, and the dimensionality D. While in this paper we focused on the case of spinless fermions, these results hold for any type of many-

body statistics, such as spinful fermions or bosons. Indeed, the existence of nonconducting channels and the percolation bound on the transition both rely on the presence of blocking unit cells in the network. In Hamiltonian $\hat{\mathcal{H}}$ (1), cells with zero particles $\hat{I}_{\mathbf{l}} = 0$ are always blocking irrespective of the statistics of the particles considered. This holds even in those cases, e.g., bosons, where the maximum occupation of a cell is not limited.

Our analysis—rooted in geometric percolation theory, alongside recent findings of localization-delocalization transition in 2D quantum link models [19]—highlights classes of disorder-free many-body quantum systems in one and higher spatial dimensions where any type of transport is completely suppressed for any filling fraction δ. Exploring these quantum effects and investigating the distinction between classical and quantum percolation transitions [63,64] are crucial future developments, which may have important repercussions for the research in the field of quantum transport. These results and open quests emphasize MBFBL networks as experimentally realizable [65–67], valid platforms to explore novel phenomena in quantum systems, highlighting jointly with Refs. [32–43] the progressively growing relevance of flat bands in the realm of many-body physics.

Acknowledgments. This work was supported by the Institute for Basic Science (Project No. IBS-R024-D1). We thank Ivan Khaymovich for helpful discussions.

[1] L. Fleishman and P. W. Anderson, Interactions and the Anderson transition, Phys. Rev. B **21**, 2366 (1980).
[2] B. L. Altshuler, Y. Gefen, A. Kamenev, and L. S. Levitov, Quasiparticle Lifetime in a Finite System: A Nonperturbative Approach, Phys. Rev. Lett. **78**, 2803 (1997).
[3] Ph. Jacquod and D. L. Shepelyansky, Emergence of Quantum Chaos in Finite Interacting Fermi Systems, Phys. Rev. Lett. **79**, 1837 (1997).
[4] I. V. Gornyi, A. D. Mirlin, and D. G. Polyakov, Interacting Electrons in Disordered Wires: Anderson Localization and Low-*t* Transport, Phys. Rev. Lett. **95**, 206603 (2005).
[5] D. M. Basko, I. L. Aleiner, and B. L. Altshuler, Metal–insulator transition in a weakly interacting many-electron system with localized single-particle states, Ann. Phys. (Amsterdam) **321**, 1126 (2006).
[6] D. A. Abanin and Z. Papić, Recent progress in many-body localization, Ann. Phys. (Berlin) **529**, 1700169 (2017).
[7] D. A. Abanin, E. Altman, I. Bloch, and M. Serbyn, Colloquium: Many-body localization, thermalization, and entanglement, Rev. Mod. Phys. **91**, 021001 (2019).
[8] M. Schiulaz, A. Silva, and M. Müller, Dynamics in many-body localized quantum systems without disorder, Phys. Rev. B **91**, 184202 (2015).
[9] M. van Horssen, E. Levi, and J. P. Garrahan, Dynamics of many-body localization in a translation-invariant quantum glass model, Phys. Rev. B **92**, 100305(R) (2015).
[10] M. Pino, L. B. Ioffe, and B. L. Altshuler, Nonergodic metallic and insulating phases of Josephson junction chains, Proc. Natl. Acad. Sci. USA **113**, 536 (2016).
[11] J. M. Hickey, S. Genway, and J. P. Garrahan, Signatures of many-body localisation in a system without disorder and the relation to a glass transition, J. Stat. Mech.: Theory Exp. (2016) 054047.
[12] R. Mondaini and Z. Cai, Many-body self-localization in a translation-invariant Hamiltonian, Phys. Rev. B **96**, 035153 (2017).
[13] M. Schulz, C. A. Hooley, R. Moessner, and F. Pollmann, Stark Many-Body Localization, Phys. Rev. Lett. **122**, 040606 (2019).
[14] A. Smith, J. Knolle, D. L. Kovrizhin, and R. Moessner, Disorder-Free Localization, Phys. Rev. Lett. **118**, 266601 (2017).
[15] A. Smith, J. Knolle, R. Moessner, and D. L. Kovrizhin, Absence of Ergodicity without Quenched Disorder: From Quantum Disentangled Liquids to Many-Body Localization, Phys. Rev. Lett. **119**, 176601 (2017).
[16] A. Smith, J. Knolle, R. Moessner, and D. L. Kovrizhin, Dynamical localization in $\mathbb{Z}_2$ lattice gauge theories, Phys. Rev. B **97**, 245137 (2018).
[17] M. Brenes, M. Dalmonte, M. Heyl, and A. Scardicchio, Many-Body Localization Dynamics from Gauge Invariance, Phys. Rev. Lett. **120**, 030601 (2018).
[18] O. Hart, S. Gopalakrishnan, and C. Castelnovo, Logarithmic Entanglement Growth from Disorder-Free Localization in the Two-Leg Compass Ladder, Phys. Rev. Lett. **126**, 227202 (2021).
[19] P. Karpov, R. Verdel, Y.-P. Huang, M. Schmitt, and M. Heyl, Disorder-Free Localization in an Interacting 2D Lattice Gauge Theory, Phys. Rev. Lett. **126**, 130401 (2021).
[20] T. B. Wahl, A. Pal, and S. H. Simon, Signatures of the many-body localized regime in two dimensions, Nat. Phys. **15**, 164 (2019).
[21] J.-Y. Choi, S. Hild, J. Zeiher, P. Schauß, A. Rubio-Abadal, T. Yefsah, V. Khemani, D. A. Huse, I. Bloch, and C. Gross, Exploring the many-body localization transition in two dimensions, Science **352**, 1547 (2016).
[22] T. Thiery, F. Huveneers, M. Müller, and W. De Roeck, Many-Body Delocalization as a Quantum Avalanche, Phys. Rev. Lett. **121**, 140601 (2018).
[23] S. Gopalakrishnan and D. A. Huse, Instability of many-body localized systems as a phase transition in a nonstandard thermodynamic limit, Phys. Rev. B **99**, 134305 (2019).
[24] E. V.H. Doggen, I. V. Gornyi, A. D. Mirlin, and D. G. Polyakov, Slow Many-Body Delocalization beyond One Dimension, Phys. Rev. Lett. **125**, 155701 (2020).
[25] W. De Roeck and F. Huveneers, Stability and instability towards delocalization in many-body localization systems, Phys. Rev. B **95**, 155129 (2017).
[26] O. Derzhko, J. Richter, and M. Maksymenko, Strongly correlated flat-band systems: The route from Heisenberg spins to Hubbard electrons, Int. J. Mod. Phys. B **29**, 1530007 (2015).
[27] D. Leykam, A. Andreanov, and S. Flach, Artificial flat band systems: from lattice models to experiments, Adv. Phys. X **3**, 1473052 (2018).
[28] D. Leykam and S. Flach, Photonic flatbands, APL Photonics **3**, 070901 (2018).

[29] J. Vidal, R. Mosseri, and B. Douçot, Aharonov-Bohm Cages in Two-Dimensional Structures, Phys. Rev. Lett. **81**, 5888 (1998).

[30] J. Vidal, B. Douçot, R. Mosseri, and P. Butaud, Interaction Induced Delocalization for Two Particles in a Periodic Potential, Phys. Rev. Lett. **85**, 3906 (2000).

[31] B. Douçot and J. Vidal, Pairing of Cooper Pairs in a Fully Frustrated Josephson-Junction Chain, Phys. Rev. Lett. **88**, 227005 (2002).

[32] M. Tovmasyan, S. Peotta, L. Liang, P. Törmä, and S. D. Huber, Preformed pairs in flat Bloch bands, Phys. Rev. B **98**, 134513 (2018).

[33] S. Tilleke, M. Daumann, and T. Dahm, Nearest neighbour particle-particle interaction in fermionic quasi one-dimensional flat band lattices, Z. Naturforsch., A: Phys. Sci. **75**, 393 (2020).

[34] C. Danieli, A. Andreanov, T. Mithun, and S. Flach, Quantum caging in interacting many-body all-bands-flat lattices, Phys. Rev. B **104**, 085132 (2021).

[35] O. Hart, G. De Tomasi, and C. Castelnovo, From compact localized states to many-body scars in the random quantum comb, Phys. Rev. Research **2**, 043267 (2020).

[36] P. A. McClarty, M. Haque, A. Sen, and J. Richter, Disorder-free localization and many-body quantum scars from magnetic frustration, Phys. Rev. B **102**, 224303 (2020).

[37] Y. Kuno, T. Mizoguchi, and Y. Hatsugai, Flat band quantum scar, Phys. Rev. B **102**, 241115(R) (2020).

[38] M. Daumann, R. Steinigeweg, and T. Dahm, Many-body localization in translational invariant diamond ladders with flat bands, arXiv:2009.09705.

[39] R. Khare and S. Choudhury, Localized dynamics following a quantum quench in a non-integrable system: an example on the sawtooth ladder, J. Phys. B: At. Mol. Opt. Phys. **54**, 015301 (2020).

[40] C. Danieli, A. Andreanov, and S. Flach, Many-body localization transition from flatband fine-tuning, arXiv:2104.11055.

[41] C. Danieli, A. Andreanov, and S. Flach, Many-body flatband localization, Phys. Rev. B **102**, 041116(R) (2020).

[42] Y. Kuno, T. Orito, and I. Ichinose, Flat-band many-body localization and ergodicity breaking in the Creutz ladder, New J. Phys. **22**, 013032 (2020).

[43] T. Orito, Y. Kuno, and I. Ichinose, Exact projector Hamiltonian, local integrals of motion, and many-body localization with symmetry-protected topological order, Phys. Rev. B **101**, 224308 (2020).

[44] Let us observe that if H_0 in Eq. (1) is diagonal, then every particle-number operator $\hat{n}_{\mathbf{l},a}$ for any $\mathbf{l}$ and a is conserved—hence fully suppressing heat transport as well.

[45] C. Danieli, A. Andreanov, T. Mithun, and S. Flach, Nonlinear caging in all-bands-flat lattices, Phys. Rev. B **104**, 085131 (2021).

[46] R. B. Stinchcombe, Ising model in a transverse field. I. Basic theory, J. Phys. C: Solid State Phys. **6**, 2459 (1973).

[47] In Eq. (3) we neglected the constant energy shift terms, which do not impact the dynamics of the system.

[48] For a nonblocked island with $1 \leqslant l \leqslant M$ nonblocking cells, the boundary terms in Eq. (3) read $\frac{1}{4}[(\hat{I}_0 - 1)\hat{\sigma}_1^z + (1 - \hat{I}_{M+1})\hat{\sigma}_M^z]$, where $\hat{I}_0, \hat{I}_{M+1}$ are the particle-number operators in unit cells $l = 0, M + 1$.

[49] K.-W. Sun, C. Wang, and Q.-H. Chen, Heat transport in an open transverse-field Ising chain, Europhys. Lett. **92**, 24002 (2010).

[50] The two forms of H_0 are equal for specific cases, e.g., with constant diagonal entries s and equal nonzero off-diagonal entries t.

[51] Y. Bar Lev, D. R. Reichman, and Y. Sagi, Many-body localization in system with a completely delocalized single-particle spectrum, Phys. Rev. B **94**, 201116(R) (2016).

[52] H. Duminil-Copin, Sixty years of percolation, in *Proceedings of the International Congress of Mathematicians (ICM 2018)* (World Scientific, Singapore, 2019), pp. 2829–2856.

[53] A. A. Saberi, Recent advances in percolation theory and its applications, Phys. Rep. **578**, 1 (2015).

[54] Again, we note that transport is not guaranteed in the nonblocked regime for reasons discussed below and similar to the 1D case.

[55] J. L. Jacobsen, Critical points of Potts and O(N) models from eigenvalue identities in periodic Temperley–Lieb algebras, J. Phys. A: Math. Theor. **48**, 454003 (2015).

[56] P. N. Suding and R. M. Ziff, Site percolation thresholds for archimedean lattices, Phys. Rev. E **60**, 275 (1999).

[57] M. Majewski and K. Malarz, Square lattice site percolation thresholds for complex neighbourhoods, Acta Phys. Pol., B **38**, 2191 (2007).

[58] O. Melchert, H. G. Katzgraber, and M. A. Novotny, Site- and bond-percolation thresholds in $K_{n,n}$-based lattices: Vulnerability of quantum annealers to random qubit and coupler failures on chimera topologies, Phys. Rev. E **93**, 042128 (2016).

[59] S. Smirnov, Critical percolation in the plane: conformal invariance, Cardy's formula, scaling limits, C. R. Seances Acad. Sci., Ser. I: Math. **333**, 239 (2001).

[60] J. Tran, T. Yoo, S. Stahlheber, and A. Small, Percolation thresholds on three-dimensional lattices with three nearest neighbors, J. Stat. Mech.: Theory Exp. (2013) P05014.

[61] T. Y. Yoo, J. Tran, S. P. Stahlheber, C. E. Kaainoa, K. Djepang, and A. R. Small, Site percolation on lattices with low average coordination numbers, J. Stat. Mech.: Theory Exp. (2014) P06014.

[62] H. J. Herrmann and H. E. Stanley, Building Blocks of Percolation Clusters: Volatile Fractals, Phys. Rev. Lett. **53**, 1121 (1984).

[63] Y. Meir, A. Aharony, and A. B. Harris, Quantum percolation, in *Scaling Phenomena in Disordered Systems* (Springer, New York, 1991), pp. 381–385.

[64] G. Schubert and H. Fehske, Quantum percolation in disordered structures, in *Quantum and Semi-classical Percolation and Breakdown in Disordered Solids* (Springer, New York, 2009), pp. 1–28.

[65] K. Fang, Z. Yu, and S. Fan, Realizing effective magnetic field for photons by controlling the phase of dynamic modulation, Nat. Photonics **6**, 782 (2012).

[66] S. Mukherjee, M. Di Liberto, P. Öhberg, R. R. Thomson, and N. Goldman, Experimental Observation of Aharonov-Bohm Cages in Photonic Lattices, Phys. Rev. Lett. **121**, 075502 (2018).

[67] S. Gladchenko, D. Olaya, E. Dupont-Ferrier, B. Douçot, L. B. Ioffe, and M. E. Gershenson, Superconducting nanocircuits for topologically protected qubits, Nat. Phys. **5**, 48 (2009).